

The Potential of Electrospun Carbon Allotrope Nanofiber Coatings in Antimicrobial Bandages

Maria-Roxana MARINESCU¹, Ioan Valentin TUDOSE^{1,2,3}, Cristina Ionela PACHIU^{1,*}, Oana BRÎNCOVEANU¹, Cosmin ROMANIȚAN¹, Mirela Petruța ȘUCHEA^{1,2}, Emmanuel KOUDOUMAS^{1,2}, and Gabriela ISOPENCU⁴

¹National Institute for Research and Development in Microtechnologies-IMT Bucharest, 126A, Erou Iancu Nicolae Street, 077190 Voluntari-Bucharest, Romania

²Center of Materials Technology and Photonics and Innovation Center (PEK), Hellenic Mediterranean University (HMU), 71410 Heraklion, Greece

³Chemistry Department, University of Crete, 70013, Heraklion, Greece

⁴National University of Science and Technology Politehnica Bucharest, 060042 Bucharest, Romania

roxana.marinescu@imt.ro, tudose.valentin@yahoo.com,
crisrina.pachiu@imt.ro*, oana.brincoveanu@imt.ro,
cosmin.romanitan@imt.ro, mirela.sucnea@imt.ro,
gabriela.isopencu@upb.ro, koudoumas@imt.ro

* Corresponding author

Abstract. Effective antimicrobial wound dressings must combine structural stability, controlled moisture management, and sustained antibacterial activity without releasing free nanoparticles into the wound. Here, electrospun polyvinylpyrrolidone (PVP) nanofiber coatings incorporating three carbon allotropes—graphene nanoplatelets (GNPs), multi-walled carbon nanotubes (MWCNTs), and nanodiamonds (NDs)—were directly deposited onto commercial medical gauze under identical fabrication conditions. This comparative design enabled systematic evaluation of how allotrope geometry and bonding structure affect nanofiber morphology, structural organization, and antimicrobial performance. This paper presents a detailed investigation of Scanning Electron Microscopy (SEM), X-Ray Diffraction (XRD), and Raman Spectroscopy, that confirmed successful incorporation of the nanocarbons within the PVP matrix while preserving the crystalline structure of the cellulose substrate. Differences in fiber diameter and structural features reflected variations in filler geometry and dispersion within the polymer network. The electrospun architecture ensured effective immobilization of nanofillers within a continuous fibrous coating firmly adhered to the textile. Antimicrobial activity, assessed by agar diffusion against *Escherichia coli*, *Bacillus subtilis*, and *Candida albicans*, showed allotrope-dependent behavior. The MWCNTs composite exhibited moderate antibacterial activity against both bacterial strains, NDs showed selective action mainly against Gram-negative bacteria, and GNPs produced no measurable inhibition. The reported results have proven that the performance of the wound dressing materials depended strongly on carbon type and structural integration within the fibrous matrix.

Key-words: Antimicrobial bandages; carbon nanomaterials; electrospun.

1. Introduction

Effective wound management remains a significant challenge in modern healthcare, particularly in the context of infection control and the increasing demand for multifunctional dressings capable of accelerating tissue regeneration while preventing microbial colonization. Advanced wound dressings are expected to provide biocompatibility, mechanical stability, moisture balance, and antimicrobial activity in a single platform [1, 2]. Electrospinning has emerged as a versatile and scalable technique for the fabrication of nanofibrous membranes characterized by high surface area, tunable porosity, and morphological similarity to the extracellular matrix [3]. Such features make electrospun systems particularly suitable for wound healing applications. The incorporation of carbon-based nanomaterials into electrospun polymer matrices has attracted considerable attention due to their multifunctional properties, including mechanical reinforcement, electrical conductivity, and reported antimicrobial activity [4, 5]. Graphene nanoplatelets (GNPs), multi-walled carbon nanotubes (MWCNTs), and nanodiamonds (NDs) represent structurally distinct carbon allotropes with fundamentally different geometries and bonding configurations. Graphene-based materials have been widely explored for wound dressings due to their hydrophilicity, mechanical strength, and reported antimicrobial behavior [6–8]. Functionalized carbon nanotubes have been investigated for biomedical applications owing to their electrical conductivity and potential to stimulate cellular responses [9]. Nanodiamonds, although less commonly employed in antimicrobial dressings, exhibit excellent chemical stability, surface tunability, and reported low cytotoxicity, making them promising candidates for biomedical coatings [10, 11]. Recent studies have demonstrated antibacterial performance of electrospun polymer matrices incorporating CNTs or graphene derivatives [12–15], supporting the feasibility of carbon-based nanofibrous wound dressing systems. Despite these advances, most existing studies focus on a single type of carbon nanomaterial under specific fabrication conditions. In particular, a systematic analysis correlating allotrope geometry (planar, tubular, quasi-spherical), bonding structure (sp^2 vs. sp^3), nanofiber morphology, structural integration, and antibacterial response has not been sufficiently clarified. Electrospinning onto textile substrates is a known strategy for advanced wound dressing architectures; however, direct comparative studies in which structurally distinct carbon allotropes are incorporated into the same polymer matrix and deposited under identical electrospinning conditions onto gauze substrates were not previously reported. Another important consideration concerns safety. The direct use of free nanoparticles in wound care raises concerns regarding potential particle release and unintended exposure. Immobilizing nanofillers within electrospun fibers directly deposited onto textile substrates offers a strategy to reduce nanoparticle mobility while maintaining functional surface exposure. Such immobilization approaches are increasingly explored in antibacterial electrospun systems [12–14], yet the relationship between structural incorporation, fiber morphology, and antimicrobial performance requires further elucidation.

In the present paper, electrospun PVP nanofiber coatings incorporating carbon allotropes were directly deposited onto commercial gauze substrates under identical fabrication conditions. This design enables a controlled comparative evaluation of how carbon allotrope type influences nanofiber diameter, crystalline behavior, vibrational signatures, and antibacterial performance. Structural characterization was carried out using scanning electron microscopy (SEM), X-ray diffraction (XRD), and Raman spectroscopy to probe both long-range crystalline order and local bonding structure [16]. Antimicrobial activity was assessed against representative Gram-negative bacteria (*Escherichia coli*), Gram-positive bacteria (*Bacillus subtilis*), and the unicellular fungus *Candida albicans*. By correlating morphological, structural, and biological results, this work

aims to clarify the role of carbon allotrope geometry and bonding configuration in determining the functional behavior of electrospun textile coatings. Compared to our previous CAS 2025 paper [16], which focused on the fabrication and preliminary structural characterization of electrospun carbon-based nanofiber coatings, the present paper provides a systematic comparative analysis under identical conditions and includes a detailed correlation between structural features and antimicrobial performance. Section 2 presents the materials, preparation methods, and electrospinning process used to fabricate the nanofiber coatings. Section 3 includes the results and discussion, covering morphological, structural, and Raman characterization, as well as antimicrobial activity evaluation. Section 4 summarizes the main findings and highlights the potential of these materials for antimicrobial wound dressing applications.

Overall, the paper provides a comparative framework for the rational design of immobilized carbon-based antimicrobial wound dressing materials.

2. Experimental Details

Polyvinylpyrrolidone (PVP, $M_w = 1,300,000$), hexadecyltrimethylammonium bromide (CTAB), and nanodiamonds (NDs; ~ 65 nm average particle size, dodecane-functionalized, powder form) were purchased from Sigma-Aldrich, while graphene nanoplatelets (GNPs; ~ 5 μm lateral size, 5 nm thickness) and multi-walled carbon nanotubes (MWCNTs; ~ 10 nm average diameter, ~ 1.5 μm average length, $\sim 95\%$ carbon purity, $<1\%$ transition metal oxides, 250–300 m^2/g BET surface area, $\sim 10^{-4}$ $\Omega\cdot\text{cm}$ volume resistivity) were supplied by Emfutur (Spain).

Three electrospinning precursor solutions were prepared, each consisting of 0.05 g of the respective carbon allotrope dispersed in a 10 g PVP solution. The samples were labeled as follows: P1 – GNPs/PVP; P2 – MWCNTs/PVP; and P3 – NDs/PVP. For the MWCNTs-based formulation (P2), 0.05 g CTAB was additionally incorporated as a dispersing agent to enhance carbon material stability in the polymer solution and to reduce aggregation associated with their high aspect ratio. All suspensions were homogenized by ultrasonication prior to electrospinning. The prepared dispersions were loaded into 10 mL syringes fitted with stainless steel needles and processed using a Nano Fiberlabs E05 electrospinning system. Electrospinning was performed at an applied voltage of 30 kV, and a needle-to-collector distance of 25 cm. The nanofibrous coatings were directly deposited onto commercial medical gauze mounted on a rotating cylindrical collector. A schematic representation of the electrospinning setup is shown in Fig. 1.

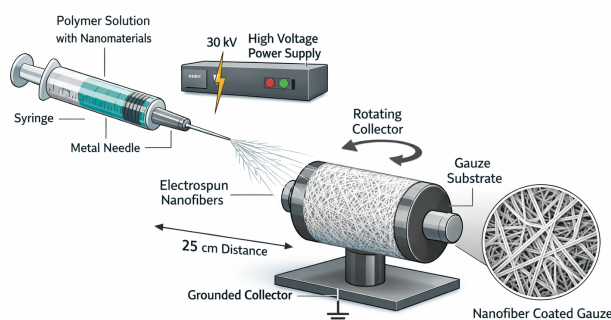


Fig. 1. Schematic representation of the electrospinning process.

Fig. 2 illustrates the in situ electrospinning process. On the left side, the pumping system is

shown, consisting of a syringe filled with the prepared polymer solution for nanofiber fabrication, along with the high-voltage cable. On the right side, the round collector is visible, featuring the gauze bandage substrate onto which the nanofibers are deposited.



Fig. 2. a) The electrospinning system Nano Fiberlabs E05; b) The bandage after the process is done.

After the process was done, the materials underwent morphological and structural characterization.

3. Results and Discussion

Electrospun nanofibers containing carbon allotropes were successfully deposited onto medical gauze substrates, forming uniform coatings with distinct morphological and structural characteristics. Morphological and structural features were assessed by SEM, XRD, and Raman Spectroscopy to validate the integration of nanomaterials into the polymer matrix.

3.1. Material morphological and structural characterization

Morphological investigations were conducted using a Nova NanoSEM 630 field-emission scanning electron microscope (FEI), operated under high-vacuum conditions. The microstructural features of the electrospun coatings, including fiber diameter distribution, surface morphology, and dispersion of carbon allotropes within the polymer matrix, were analyzed from representative micrographs acquired at different magnifications. Phase identification and structural analysis were performed by X-ray diffraction (XRD) using a Rigaku SmartLab diffractometer. Diffraction patterns were recorded in $\theta-2\theta$ configuration over an appropriate angular range to evaluate the crystalline contributions of the incorporated carbon allotropes and to assess any structural modifications induced by the electrospinning process. Raman spectroscopy measurements were carried out using a WITec Alpha 300S confocal Raman system equipped with a 532 nm excitation laser. The spectra were collected to investigate the structural characteristics of the carbon allotropes, including disorder-related and graphitic vibrational modes, and to evaluate their dispersion and interaction within the electrospun nanofibers.

3.1.1. SEM analysis

Macroscopic inspection (Fig. 3 - top row) indicates uniform deposition of nanofibrous coatings on the gauze substrate for all formulations. No visible delamination or macroscopic inhomogeneities are observed. Scanning Electron Microscopy (SEM) revealed the successful formation of continuous nanofibrous coatings on the gauze substrate for all investigated formulations. In Fig. 3 are presented photos and SEM images of the morphological characterizations of

the materials. At low magnification, homogeneous coverage of the textile fibers was observed, indicating stable electrospinning conditions and good adhesion of the nanofiber layer to the substrate. Higher-magnification micrographs highlighted a randomly oriented fibrous network with no evident bead formation, confirming stable jet elongation during deposition process.

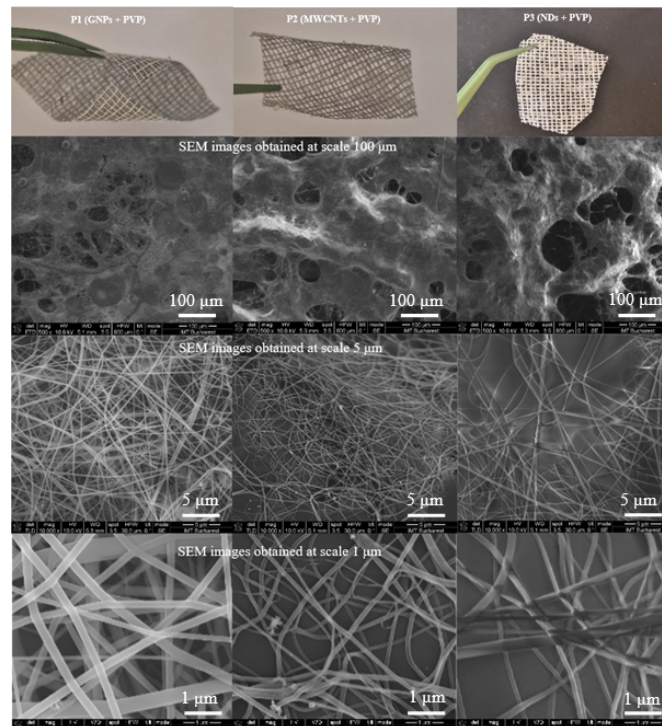


Fig. 3. Photos and SEM images of the samples.

Based on image analysis of representative SEM micrographs, the average fiber diameters were estimated to be approximately 120 nm for the GNPs/PVP sample (P1), 50–70 nm for the MWCNTs/PVP sample (P2), and 70–130 nm for the NDs/PVP sample (P3). Fiber diameters were estimated from at least 50 fibers per sample using image analysis with Image J software. The MWCNTs-containing formulation produced comparatively thinner fibers, which may be attributed to enhanced charge transport and jet stretching effects associated with the high aspect ratio and electrical conductivity of the multi-walled nanotubes. In contrast, the GNPs-based formulation exhibited moderately larger fiber diameters, potentially reflecting increased solution viscosity and altered flow dynamics due to the incorporation of platelet-like fillers. The NDs/PVP sample displayed intermediate behavior, consistent with the spherical morphology of the nanoparticles and their comparatively lower influence on elongational flow during electrospinning. Overall, the SEM analysis confirms that the incorporation of different carbon allotropes influences fiber morphology and diameter distribution under otherwise identical processing conditions.

3.1.2. XRD analysis

Fig. 4 presents the X-ray diffraction (XRD) patterns of the electrospun nanofiber-coated gauze samples (P1–P3), together with the corresponding reference patterns of graphite, MWCNTs, and diamond.

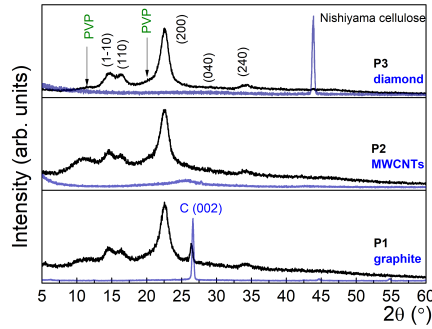


Fig. 4. XRD patterns for P1: GNPs/PVP, P2: MWCNTs/PVP and P3: ND/PVP.

The diffraction maxima located at approximately $2\theta = 14.6^\circ$, 16.4° , 22.5° , 28.8° , and 33.4° were assigned to the $(1\bar{1}0)$, (110) , (200) , (040) , and (240) reflections of cellulose $I\beta$, in agreement with the crystallographic data reported by Nishiyama *et al.* [17] and analyzed by French [18]. These reflections confirm that the crystalline structure of the cellulose gauze substrate is preserved after electrospinning and nanomaterial deposition. Since electrospinning was performed as a surface coating process, no structural modification of the underlying cellulose substrate is expected.

Additional weak reflections observed at $2\theta \approx 10.9^\circ$ and 20.1° were attributed to residual PVP contributions from the polymeric matrix. For sample P1 (GNPs/PVP), an additional diffraction peak located at $2\theta \approx 26.4^\circ$ is observed and assigned to the (002) planes of graphitic carbon, confirming the incorporation of graphene nanoplatelets within the nanofiber network. In contrast, no distinct diffraction peaks attributable to MWCNTs (P2) or nanodiamond (P3) were clearly resolved. This may be attributed to the relatively low filler concentration and to the partial overlap between carbon-related reflections and the broad cellulose (200) peak centered at $\sim 22\text{--}23^\circ$. Moreover, nanoscale dispersion and limited coherent domain size of the incorporated nanomaterials can significantly reduce diffraction intensity. Therefore, the absence of sharp characteristic reflections does not exclude their presence but rather suggests homogeneous dispersion within the composite matrix. The crystallinity index (CrI) of cellulose was evaluated using Segal's empirical relation [19], applying identical background subtraction and data treatment procedures for all samples to ensure consistency:

$$CrI(\%) = \frac{I_{200} - I_{am}}{I_{200}} \times 100 \quad (1)$$

where I_{200} is the diffraction intensity of the (200) reflection, while I_{am} is the intensity at the minimum between (110) and (200) . The calculated crystallinity indices were approximately 76% (P1), 78% (P2), and 86% (P3). Since the electrospinning process does not modify the cellulose substrate structure, the observed variations in CrI are attributed primarily to differences in relative peak intensity contributions and potential changes in scattering contrast induced by

the incorporated carbon allotropes. The higher apparent crystallinity for P3 may reflect reduced overlap between nanodiamond scattering and cellulose reflections compared to the other carbon fillers. As cellulose crystallinity is closely correlated with mechanical rigidity and structural organization [20,21], these variations may affect the mechanical response of the coated dressings. However, the overall cellulose I β structure remains unchanged across all samples.

3.1.3. Raman spectroscopy analysis

Raman spectroscopy (Fig. 5) was employed to investigate the structural characteristics of the carbon allotropes incorporated into the polyvinylpyrrolidone (PVP) nanofibrous matrix.

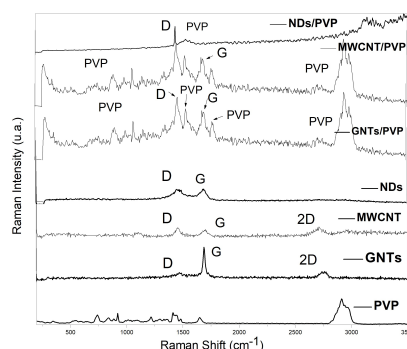


Fig. 5. Raman spectra for P1: GNPs/PVP, P2: MWCNTs/PVP, and P3: NDs/PVP.

The reference spectra of pristine GNPs and MWCNTs exhibit the characteristic carbon-related vibrational features, including the D band (1350 cm^{-1}), associated with defect-activated breathing modes of sp^2 carbon rings, and the G band (1580 cm^{-1}), corresponding to the in-plane stretching vibration of sp^2 -hybridized carbon atoms [22, 23]. In addition, the presence of the 2D band in the $2660\text{--}2700\text{ cm}^{-1}$ region confirms the graphitic nature of these nanomaterials [24]. For both GNPs/PVP and MWCNTs/PVP composites, the D and G bands remain clearly visible, demonstrating that the structural framework of the carbon allotropes is preserved after electrospinning and incorporation into the polymer matrix. The relative enhancement of the D band intensity compared to the G band (I_D/I_G ratio) suggests the presence of structural disorder, which may arise from edge defects, intrinsic lattice imperfections, or interfacial interactions between the carbon nanofillers and PVP chains. Such behavior is commonly observed in polymer-carbon nanocomposites and may indicate partial perturbation of the graphitic domains due to processing or dispersion within the matrix. The 2D band remains detectable in both composites, although with reduced intensity compared to the precursor fillers, which is consistent with multilayer GNPs and MWCNTs embedded in a polymer environment. In contrast, the Raman spectrum of the NDs/PVP composite exhibits a markedly different response. A weak feature near 1332 cm^{-1} can be attributed to the first-order Raman mode of sp^3 -bonded carbon characteristic of diamond structures [25]. However, the relatively low intensity of this band, combined with the dominant polymer background, suggests either a reduced Raman scattering cross-section of nanodiamonds or strong matrix-related signal overlap. This attenuation effect is frequently reported in nanodiamond-polymer systems and may be influenced by particle size, surface functionalization, and dispersion state. The distinct Raman signatures observed for the three carbon allotropes reflect their intrinsic structural differences and confirm their successful

incorporation within the electrospun PVP nanofiber network. While Raman spectroscopy primarily provides structural information, the preserved carbon-related vibrational modes indicate that the nanofillers maintain their fundamental bonding configuration after processing. Given the structural differences revealed by Raman analysis, variations in functional performance can be anticipated. Graphene nanoplatelets, due to their high specific surface area and exposed edge sites, and carbon nanotubes, owing to their high aspect ratio and extended sp^2 network, are known to interact differently with biological systems [26]. Nanodiamonds, characterized predominantly by sp^3 bonding, may exhibit distinct surface reactivity depending on functional groups and defect density. Embedding these nanomaterials within a PVP matrix via electrospinning enhances their stabilization within the textile substrate and reduces the likelihood of nanoparticle detachment.

A comprehensive understanding of the structural behavior of the developed nanocomposites emerges from the combined SEM, XRD, and Raman investigations. SEM analysis revealed that the incorporation of different carbon allotropes influences the nanofiber morphology and average diameter. These variations suggest that the geometry and aspect ratio of the nanofillers affect jet stretching dynamics during electrospinning. High-aspect-ratio CNTs likely enhance charge transport and elongational forces, leading to thinner fibers, whereas platelet-like GNPs may increase effective solution viscosity, resulting in slightly thicker fibers. XRD analysis confirmed that the crystalline structure of the cellulose substrate (cellulose $I\beta$) remains unchanged after electrospinning and nanofiller incorporation. The appearance of the graphitic (002) reflection at 26.4° in P1 corroborates the presence of GNPs, in agreement with Raman observations. In contrast, the absence of well-defined MWCNT and diamond reflections in P2 and P3 is consistent with their low concentration and nanoscale dispersion within the polymer matrix, which reduces long-range coherent scattering detectable by XRD. Raman spectroscopy further supports these findings by providing local structural information on the carbon bonding configuration. The preservation of the D, G, and 2D bands in the GNPs/PVP and MWCNTs/PVP composites confirms that the sp^2 carbon framework remains intact after electrospinning. The increased I_D/I_G ratio observed in the composites suggests the presence of structural disorder and interfacial interactions between the carbon nanomaterials and the polymer chains, which may not be detectable by XRD due to its sensitivity to long-range order. For the NDs/PVP sample, the weak band near 1332 cm^{-1} attributed to sp^3 carbon is consistent with the limited diamond-related diffraction features observed in XRD.

The consistency between SEM morphology, diffraction behavior, and vibrational signatures indicates that the carbon nanomaterials are effectively embedded within the electrospun PVP network without altering the cellulose crystalline structure of the textile substrate. The observed structural differences at both nano- and micro-scale levels are expected to influence the functional behavior of the composites. This fibrous network acts as a physical immobilization matrix, limiting nanoparticle mobility while preserving the functional surface characteristics of the carbon fillers. Such immobilization strategies are increasingly adopted in the design of antibacterial materials, where nanofillers are embedded within polymeric fibers rather than applied in particulate form. This configuration is expected to improve structural stability and reduce the likelihood of nanoparticle detachment during handling or application.

3.2. Antimicrobial activity evaluation

The antimicrobial functionality of the electrospun carbon-based nanocomposites was evaluated using the agar diffusion (inoculum depletion) method against representative Gram-negative

bacteria (*Escherichia coli* DH5K strain - EC), Gram-positive bacteria (*Bacillus subtilis* var. *spizizenii* - BS), and the unicellular fungus *Candida albicans* - CA from the collection of microorganisms of the Bioreactor Laboratory, FICBi. The culture medium used was Luria Bertani (modified Miller) - agar (purchased from Roth) -LBA, a highly-referenced nutrient-rich microbial growth powder medium, suitable for regular bacterial culture and Malt Extract Agar (purchased from Roth) for fungi cultivation. Optical density (DO) of the inoculum, measured at 600 nm, represented by young cells in the exponential phase of growth was: for DO-EC=0.2755; DO-BS=0.1837; DO-CA=0.3570. The plates were inoculated with 100 mL of microbial suspension using the inoculum depletion method and left for approximately 1 hour in a humidity-controlled oven to allow uniform absorption of the suspension into the medium and to eliminate excess surface liquid. The samples were cut into 10 × 10 mm squares and sterilized under UV light (256 nm) using a Portable UV Lamp (ROTH type IV, 254/366 nm) for 30 minutes. They were then aseptically placed on the surface of the culture medium in Petri dishes. The samples were incubated at 37°C for 24 hours. All assays were conducted in triplicate to ensure reproducibility. The antimicrobial response was quantified by measuring the inhibition zone (IZ, mm) and is represented by the clear zone that differentiates around the films impregnated with the active substance, considering the real surface of film, according to the attached images from Fig. 6.

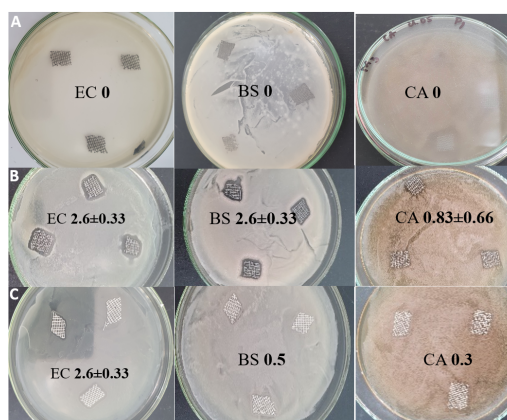


Fig. 6. A) GNPs/PVP composite (P1) – No measurable inhibition zones observed; B) MWCNTs/PVP composite (P2) – Measurable antibacterial effects; C) NDs/PVP composite (P3) – Selective antibacterial effects.

The GNPs/PVP composite (P1) did not exhibit measurable inhibition zones against any of the tested microorganisms (Fig. 6-A). Although graphene-based materials are widely reported to possess antimicrobial activity, the absence of detectable inhibition under the present conditions suggests that the effective graphene concentration and/or the exposure of active edge sites within the electrospun matrix were insufficient to generate a diffusion-based antimicrobial response. This result indicates that structural incorporation of graphene, as confirmed by Raman spectroscopy, does not automatically translate into measurable antimicrobial performance and highlights the importance of filler loading and surface accessibility.

In contrast, the MWCNTs/PVP composite (P2) demonstrated moderate antimicrobial activity against both Gram-negative and Gram-positive bacteria, with inhibition zones of 2.6 ± 0.33 mm for *E. coli* and 2.6 ± 0.33 mm for *B. subtilis*. A significantly lower antifungal activity was

observed against *C. albicans* (0.83 ± 0.66 mm) (Fig. 6-B). The comparable inhibition for Gram-negative and Gram-positive bacteria suggests that the MWCNT-mediated antimicrobial action is not strongly selective with respect to bacterial cell wall type. This behavior may be attributed to the high aspect ratio and elongated morphology of carbon nanotubes, which can promote membrane interaction and possible mechanical disruption. The reduced activity against fungi is consistent with the more complex and robust structure of eukaryotic cell membranes.

The NDs/PVP composite (P3) exhibited selective antibacterial behavior, producing an inhibition zone of 2.6 ± 0.33 mm against *E. coli*, while only weak inhibition was observed for *B. subtilis* (0.5 mm) and *C. albicans* (0.3 mm) (Fig. 6-C). The higher sensitivity of Gram-negative bacteria suggests a membrane-dependent interaction mechanism. Nanodiamond particles, characterized predominantly by sp^3 carbon bonding as confirmed by Raman analysis, may interact with microbial membranes through surface functional groups or localized oxidative processes; however, their antibacterial efficiency appears lower compared to the MWCNTs-based system, particularly against Gram-positive bacteria and fungi.

Together, these results demonstrate that the observed antimicrobial activity originates from the incorporated carbon allotropes rather than from structural modification of the underlying substrate, with the observed inhibition zones confirming the proof-of-concept functionality of MWCNTs and NDs containing electrospun coatings.

Although the antimicrobial effect is moderate, the results confirm that embedding carbon nanomaterials within a fibrous polymer matrix can generate measurable biological activity while maintaining structural integrity of the dressing material. Future work will focus on optimization of nanofiller loading and coating density, followed by more detailed investigations using quantitative methods such as minimum inhibitory concentration inhibitory assay to more accurately assess antimicrobial efficiency, and biocompatibility of the samples with the mammalian cells and those viability analyses to verify whether these materials can be used for direct tissue contact in wound treatment.

4. Conclusions

Electrospinning proved to be an effective and versatile method for the fabrication of uniform nanofiber coatings incorporating carbon-based nanomaterials directly onto textile gauze substrates. The developed approach enables controlled integration of graphene nanoplatelets, multi-walled carbon nanotubes, and nanodiamonds within a PVP matrix, forming continuous fibrous layers firmly adhered to the underlying cellulose support. Morphological (SEM), structural (XRD), and vibrational (Raman) analyses consistently confirmed the successful incorporation of the carbon allotropes while preserving the crystalline structure of the cellulose substrate. The electrospun architecture provides effective immobilization of the nanofillers within the polymer network, which is advantageous in reducing the risk of nanoparticle detachment during handling or potential wound application.

Biological evaluation using agar diffusion assays against *Escherichia coli* (Gram-negative), *Bacillus subtilis* (Gram-positive), and *Candida albicans* demonstrated that antimicrobial performance is strongly dependent on the type of carbon allotrope and its integration within the fibrous matrix. The GNP/PVP sample did not exhibit measurable inhibition under the present loading conditions, indicating that structural presence alone is insufficient to ensure antibacterial activity. In contrast, the MWCNTs-containing composite showed moderate antibacterial activity against both Gram-negative and Gram-positive bacteria, while nanodiamond-based fibers displayed se-

lective activity predominantly against Gram-negative bacteria, with limited antifungal response. These findings confirm the proof-of-concept functionality of carbon nanomaterial-based electrospun coatings for antimicrobial textile applications. Although the observed inhibition zones are moderate, the results demonstrate that immobilized carbon allotropes can generate measurable antibacterial effects without altering the structural integrity of the textile substrate. Overall, the proposed electrospinning strategy represents a scalable and tunable platform for the development of multifunctional wound dressing materials integrating structural stability with antimicrobial functionality.

Acknowledgements. This research was partially supported by the INFRACHIP EU Horizon Europe Grant No 101131822, partially funded by the Romanian Ministry of Research, Innovation and Digitalization under the Romanian National Nucleu Program μ NanoEI, project code PN 2307, contract no. 8N/03.01.2023 and partially by PNRR/2022/C9/MCID/I8CF23/14 11 2022 contract 760101/23.05.2023, financed by the Ministry of Research, Innovation and Digitalization in “Development of a program to attract highly specialized human resources from abroad in research, development, and innovation activities” within the –PNRR-IIIIC9-2022 –18 PNRR/2022/Component 9/investment8.

5. References

- [1] S. POLAKA, B. PAWAR, N. VASDEV and R. K. TEKADE, *Development and biological evaluation of smart powder bandage for wound healing and dressing applications*, International Journal of Biological Macromolecules **258**(2), 2024, paper 129044.
- [2] P. NEZHAD-MOKHTARI, E. KASHANI, M. MAZLOOMI, M. GHahremani-NASAB, I. AHADZADEH, A. RAHMANI DEL BAKHSHAYESH and H. HAMISHEHKAR, *Electroactive dopamine-functionalized reduced graphene oxide/alginate hydrogel containing thymol/chitosan nanoparticles for advanced antibacterial and bioadhesive wound dressings*, Carbohydrate Polymers **380**, 2026, paper 124960.
- [3] J. XUE, T. WU, Y. DAI and Y. XIA, *Electrospinning and electrospun nanofibers: methods, materials, and applications*, Chemical Reviews **119**(8), 2019, paper 5298–5415.
- [4] J. TANG, Y. WU, S. MA, T. YAN and Z. PAN, *Flexible strain sensor based on CNT/TPU composite nanofiber yarn for smart sports bandage*, Composites Part B: Engineering **232**, 2022, paper 109605.
- [5] J. TANG, Y. WU, S. MA, Y. ZHANG, T. YAN and Z. PAN, *Three-directional knitted fabric sensor made of elastic carbon-based nanofiber yarn with excellent tensile and pressure sensing performance*, Nano Energy Part A **128**, 2024, paper 109801.
- [6] K. SHANKAR, S. AGARWAL, S. MISHRA, P. BHATNAGAR, S. SIDDIQUI and I. ABRAR, *A review on antimicrobial mechanism and applications of graphene-based materials*, Biomaterials Advances **150**, 2023, paper 213440.
- [7] A. CUMONT, A. R. PITT, P. A. LAMBERT, M. R. OGGIONI and H. YE, *Properties, mechanism and applications of diamond as an antibacterial material*, Functional Diamond **1**(1), 2021, pp. 1–28.
- [8] I. H. ALI, A. OUF, F. ELSHISHINY, M. B. TASKIN, J. SONG, M. DONG, M. CHEN, R. SIAM and W. MAMDOUH, *Antimicrobial and wound-healing activities of graphene-reinforced electrospun chitosan/gelatin nanofibrous nanocomposite scaffolds*, ACS Omega **7**(2), 2022, pp. 1838–1850.
- [9] Y. ZHANG, Y. BAI and B. YAN, *Functionalized carbon nanotubes for potential medicinal applications*, Drug Discovery Today **15**(11–12), 2010, pp. 428–435.

- [10] H. PARK, T. V. PATIL, C. MO and L. KI-TAEK, *Nanodiamond: a multifaceted exploration of electrospun nanofibers for antibacterial and wound healing application*, Journal of Nanobiotechnology **23**(285), 2025, pp. 1–30.
- [11] A. HYDER, A. ALI, J. A. BULEDI, A. A. MEMON, M. IQBAL, T. H. BANGALNI, A. R. SOLANGI, K. H. THEBO and J. AKHTAR, *Nanodiamonds: a cutting-edge approach to enhancing biomedical therapies and diagnostics in biosensing*, Chem Record **24**(4), 2024, paper e202400006.
- [12] J. D. SCHIFFMAN and M. ELIMELECH, *Antibacterial activity of electrospun polymer mats with incorporated narrow diameter single-walled carbon nanotubes*, ACS Applied Materials & Interfaces **3**(2), 2011, pp. 462–468.
- [13] H. SHI, H. LIU, S. LUAN, D. SHI, S. YAN, C. LIU, R. K. Y. LI and J. YIN, *Effect of polyethylene glycol on the antibacterial properties of polyurethane/carbon nanotube electrospun nanofibers*, RSC Advances **6**(23), 2016, pp. 19238–19244.
- [14] S. SAMATYA YILMAZ and A. AYTAC, *Antibacterial wound dressing with cross-linked electrospun surface from reduced graphene oxide doped polyvinyl alcohol/sodium caseinate blends*, Biopolymers **115**(3), 2024, pp. e23579.
- [15] Z. ZHENG, Q. HUANG and L. LIU, *One-step electrospinning of carbon nanowebs on metallic textiles for high-capacitance supercapacitor fabrics*, Journal of Materials Chemistry A **4**(18), 2016, pp. 6802–6808.
- [16] M.-R. MARINESCU, I. V. TUDOSE, C. I. PACHIU, O. BRINCOVEANU, C. ROMANITAN, M. P. SUCHEA and E. KOUDOUMAS, *Electrospun carbon allotrope nanofiber coatings that can be used for advanced antibacterial bandages*, Proceedings of 2025 International Semiconductor Conference, Sinaia, Romania, 2025, pp. 317–320.
- [17] Y. NISHIYAMA, P. LANGAN and H. CHANZY, *Crystal structure and hydrogen-bonding system in cellulose I β from synchrotron X-ray and neutron fiber diffraction*, Journal of the American Chemical Society **124**(31), 2002, pp. 9074–9082.
- [18] F. STEVEN, *The structure of the world: Metaphysics and representation*, Oxford University Press, UK, 2014.
- [19] L. SEGAL, J. J. CREELY, A. E. MARTIN and C. M. CONRAD, *An empirical method for estimating the degree of crystallinity of native cellulose using the x-ray diffractometer*, Textile Research Journal **29**(10), 1959, pp. 786–794.
- [20] E. GÜMÜSKAYA, U. MUSTAFA and K. HÜSEYİN, *The effects of various pulping conditions on crystalline structure of cellulose in cotton linters*, Polymer Degradation and Stability **81**(3), 2003, pp. 559–564.
- [21] P. CARRIÓN-PRIETO, P. MARTIN-RAMOS, S. HERNANDEZ-NAVARRO, L. F. SANCHEZ-SASTRE, J. L. MARCOS-ROBLES and J. MARTIN-GIL, *Crystallinity of cellulose microfibers derived from *Cistus ladanifer* and *Erica arborea* shrubs*, Maderas. Ciencia y tecnología **21**(4), 2019, pp. 447–456.
- [22] A. C. FERRARI and D. M. BASKO, *Raman spectroscopy as a versatile tool for studying the properties of graphene*, Nature Nanotechnology **8**, 2013, pp. 235–246.
- [23] C. FERRARI and others, *Raman spectrum of graphene and graphene layers*, Physical Review Letters **97**, 2006, paper 187401.
- [24] M. S. DRESSELHAUS, A. JORIO, M. HOFMANN, G. DRESSELHAUS and R. SAITO, *Perspectives on carbon nanotubes and graphene Raman spectroscopy*, Nano Letters **10**, 2010, pp. 751–758.
- [25] J. PHIRI, G. PATRICK and M. THADDEUS, *High-concentration shear exfoliation of graphite into graphene using polymer stabilizers*, Journal of Materials Science **52**, 2017, pp. 8321–8337.
- [26] S. REICH and C. THOMSEN, *Raman spectroscopy of graphite*, Philosophical Transactions of the Royal Society A **362**, 2004, pp. 2271–2288.